RSC Publishing Faraday Discussions

Symmetry Breaking Charge Transfer as a Means to Study Electron Transfer With No Driving Force.

Journal:	*Faraday Discussions*
Manuscript ID	FD-ART-11-2018-000201.R1
Article Type:	Paper
Date Submitted by the Author:	17-Dec-2018

Complete List of Authors:	Kellog, Micheal; University of Southern California, Department of Chemistry Akil, Ali; University of Southern California, Department of Chemistry Sylvinson M. R., Daniel; University of Southern California, Department of Chemistry Estergreen, Laura; University of Southern California, Department of Chemistry Bradforth, Stephen; University of Southern California, Chemistry Thompson, Mark; University of Southern California, Department of Chemistry

SCHOLARONE™
Manuscripts

Symmetry Breaking Charge Transfer as a Means to Study Electron Transfer With No Driving Force.†

Michael Kellogg, Ali Akil, Daniel Sylvinson M. R., Laura Estergreen, Stephen E. Bradforth*, Mark E. Thompson*

Department of Chemistry, University of Southern California, Los Angeles, CA 90089, USA

Abstract

Symmetry breaking charge transfer (SBCT) is a process where a symmetrically disposed pair of identical chromophores forms a charge transfer excited state with the hole and electron on different chromophores, *i.e.* chr-chr +hν → chr^{+}-chr^{-}. Herein we explore this process in two dipyrrin-based bichromophoric systems. One of these bisdipyrrins involved a pair of BODIPY chromophores linked by a single bond at their *meso*-positions (compound **1**) and the other involved two dipyrrin ligands coordinated in a tetrahedral geometry at the Zn^{2+} ion (compound **2**). Both compounds show rapid SBCT in polar solvents and only dipryrrin based emission in nonpolar solvents, the latter arising from a dipyrrin localized excited sate (LE). By "tuning" the solvent polarity the equilibrium between the LE and SBCT states can be shifted to favor either state. Ultrafast transient absorption spectroscopy (TA) was used to probe the kinetics of the charge transfer for **2** in solvents where the electron transfer is endergonic, exergonic and has a ΔG close to zero. Our TA derived rates were used to predict fluorescence efficiencies in each of the different solvent systems and showed a good correspondence to measured values. Detailed density functional theory (DFT) and time dependent DFT were used to model the ground states

† Electronic supplementary information (ESI) available. The ESI contains (1) xyz coordinates for the ground state, LE and SBCT excited states for **1** and **2**, (2) the solvent compositions, $E_T(30)$ and dielectric values for all of the lmixtures used here, (3) derivations of equations 1 and 2, (4) TA spectra for **2** in all solvents and solvent mixtures (15 total).

as well as the LE and SBCT states of **1** and **2**, in both polar and nonpolar media. The ground and LE excited states show small dipole moments, while the SBCT states show dipole moments of 16.4 and 20.3 D for **1** and **2**, respectively.

Introduction

The simplest way to form a charge separated excited state in a molecular chromophore is to link an electron donor to an acceptor so that an intramolecular charge transfer (ICT) state is formed upon irradiation. Strong coupling of D-A groups gives a good oscillator strength for the CT transition, but lowers the energy of the ICT state relative to the singlet energy of either the donor or acceptor. This limits the available oxidization and reduction potential available from the ICT state to be well below that of the oxidized donor or reduced acceptor alone, respectively. Linking two dye molecules into a non-polar symmetric pair that are only weakly coupled is an alternate approach to promote charge separation (Figure 1). An example of this occurs in the bacterial photosynthetic reaction centre, where two bacteriochlorophylls are spatially close, but weakly interacting, to form the "special pair". After bacteriochlorophylls are optically excited, ultrafast formation of an intradimer CT state is observed.[1] This approach leads to rapid (*i.e.* ps time scale) charge separation with an energy loss between

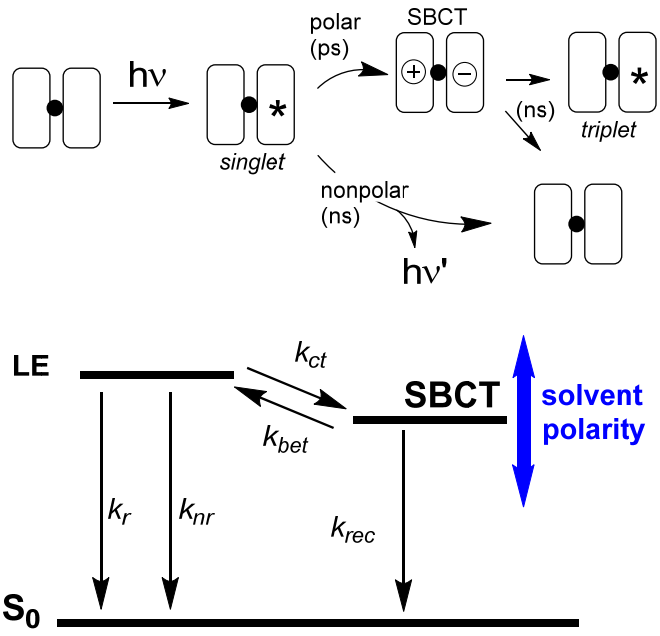

Figure 1: (top) A schematic representation of the decay process for SBCT materials in polar and non-polar media. Two identical chromophores are represented by the open rectangles and the asterisk indicates an excited chromophore (singlet or triplet). (bottom) A kinetic scheme is shown for the SBCT process. The energy of the CT state is strongly solvent independent, while that of the chromophore localized singlet (labelled LE) is largely solvent independent.

the exciton and charge separated state of <100 mV.[2] This rapid formation of the SBCT state is especially useful for red and NIR excited states, such as those of bacteriochlorophylls, since this will efficiently outcompete fluorescence or nonradiative decay from the singlet excited state.

The small energy loss in charge separation in SBCT is in contrast to the typically offset of 500 mV or more between the singlet energy of the donor or acceptor and D^+/A^-, used to promote rapid intramolecular charge transfer. As previously noted by Rettig,[3] symmetry-breaking CT states facilitate charge separation with minimal energy loss, and simultaneously slow recombination rates for systems with orthogonal chromophores, both of which are beneficial in in a wide range of applications, from photo-electro-catalysis and photovoltaics to photodynamic therapy. We have recently shown that SBCT can be used to significantly enhance the open circuit voltage of organic solar cells,[4] by increasing the rate of charge transfer between donor and acceptors layers in the devices. Symmetry-breaking charge transfer is proposed to occur in any symmetric molecular dyad provided: (1) the energy of the singlet state for the monomeric component of the dyad is nearly degenerate with or greater than that of redox gap ($\Delta E_{redox} = E_{1/2}^{ox} - E_{1/2}^{red}$), (2) the chromophores are spatially oriented to minimize both orbital and exciton coupling, and (3) the chromophores are close enough to undergo rapid electron transfer. Until recently, model compounds capable of SBCT have been largely confined to bi-acenes that absorb light at predominantly ultraviolet wavelengths.[3, 5-7] The 9,9'-bianthryl molecule is the best studied system of this sort, and the emissive nature of its excited state provides a useful probe to study the nature of SBCT.[8-10]

The approach used to generate chromophore dimers suitable for SBCT has involved coupling two planar chromophores such that steric constraints force them to be are orthogonal to each other. This geometry guarantees minimal overlap of their wavefunctions in the ground state or of the hole and electron formed in SBCT. The orthogonal geometry leads to a very small exchange energy for the singlet and triplet states and thus acts as an efficient intermediate state for the

formation of the chromophore localized triplet (Figure 1).[11] This efficient triplet formation has been used to efficiently sensitize singlet oxygen, *i.e.* chr-chr + hν → ^{1}chr-chr → ^{1,3}(chr$^+$-chr$^-$) → ^{3}chr-chr + $^1O_2$ → chr-chr + $^3O_2$ (chr = chromophore) and been proposed as a heavy metal free photodynamic therapy agent.[12-14] It is important to note that the SBCT state lives for nanoseconds before decaying to the chromophore localized triplet in the absence of oxygen and can be used to drive redox reactions at oxidation and reduction potentials close to the potentials of the isolated chr$^+$ and chr$^-$ ions, respectively.

Cyanine-type dyes such as difluoroboron dipyrrins (BODIPY) have the appropriate energetics to satisfy requirement (1) above for SBCT and absorb strongly at visible wavelengths.[15] The HOMO and LUMO orbitals are shown in Figure 2 for a metal coordinated dipyrrin. The principal absorption band for these complexes involves a HOMO-LUMO transition, leading to strong absorption in the 500 nm range for a simple dialkyl-dipyrrin of the type pictured here (ε = 10^5 $M^{-1}cm^{-1}$). We have recently reported a *meso*-bridged BODIPY dimer dyad (**1** in Figure 2) that undergoes SBCT upon excitation.[16] Excitation of **1** at 500 nm leads to rapid formation of the SBCT state (< 1 ps) in polar solvents such as dichloromethane or acetonitrile. While we have not been able to get x-ray quality crystals of this compound, modeling predicts that the two dipyrrins are close to orthogonal (98°).

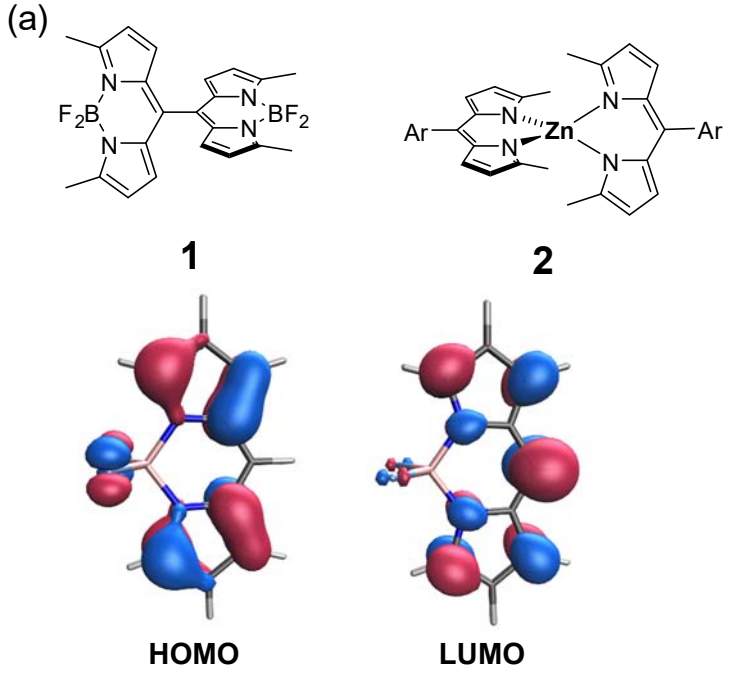

Figure 2: (a) Dipyrrin structures used to study symmetry breaking charge transfer in this paper. Ar = 1-mesityl (b) The HOMO and LUMO orbitals of BODIPY are shown. The surfaces are the same for Zn coordinated to the dipyrrin.

A second class of molecules that have the characteristics to exhibit SBCT are bis-dipyrrinato (dipy) zinc complexes such as **2**.[17, 18] In these complexes the tetrahedral coordination geometry ensures an orthogonal relationship of the two dipyrrins, minimizing the orbital overlap and exciton coupling between the two ligands. The Zn complexes are readily synthesized, absorb strongly in the visible spectrum and do in fact undergo rapid charge separation (< 5 ps), even in solvents of low polarity such as toluene.[17, 19] Interestingly, SBCT occurs despite the fact that ΔE_{redox} is greater than the singlet energy in these complexes, seemingly counter to the thermodynamic requirement (1) given above. However, charge separation is favored in this case due to the close proximity of the chromophores and the additional stabilization from the screened interaction of the charge separated pair over the cation or anion by the solvent dielectric.

The 9,9'-bianthryl molecule is probably the best studied system exhibiting SBCT, and the emissive nature of its excited state provides a useful probe to study the nature of SBCT.[8-10] 9,9'-Bianthryl has been studied through time resolved microwave conductivity,[20] dc photocurrent measurements[21] and transient absorption measurements,[22-24] The combined studies infer that the charge transfer is occurring by a through-bond mechanism where the anthracene chromophores are initially coupled by activation of a torsional mode that has the chromophores oscillating between 60° and 120° with respect to one another.[24] This torsion results in an initial partial charge transfer in all solvents, largely at the *meso*-carbons joining the two anthryl units, followed by complete interchromophore charge transfer in polar solvents, where the CT state is further stabilized. Herein we will compare the rates of SBCT between the meso-bridged BODIPY dimer and an organometallic dimer system where the through-bond mechanism is inhibited.

The energy difference between the locally excited state on the chromophore and charge transfer state is strongly solvent dependent. Both **1** and **2** give high fluorescence efficiencies in nonpolar solvents, with emission spectra nearly identical to the isolated chromophore, consistent with the SBCT state lying well above the LE state. As the polarity of the solvent is increased, the

SBCT state is stabilized to the point where it is the lowest energy excited state and its red-shifted and inefficient emission takes over (Figure 1). Using the polarity of the solvent, we can create a situation where the LE and SBCT states become degenerate, so the free energy for the charge transfer reaction is zero. In this paper we discuss these experiments, where solvent mixtures were used to "fine tune" the solvent polarity. We have measured the kinetic parameters for all of the steps outlined in the scheme in Figure 1 as a function of the solvent dielectric and will discuss them in in the context of the charge transfer process in the absence of a driving force, *i.e.* $\Delta G° = 0$. We will also discuss our molecular modeling of the LE and SBCT states for **1** and **2**, to better understand the structural and electronic changes that take place in this electron transfer process.

Results and Discussion

Electron Transfer at Zero Driving Force

By adjusting the polarity of the solvent, we can shift the energy of the SBCT states to fall above or below the LE state of **2**. The same situation exists for **1**, but we will focus solely on **2** in this section. First, we wil consider pure solvents: cyclohexane (CHX), toluene (TOL) tetrahydrofuran (THF) and acetonitrile (ACN). With cyclohexane as solvent the SBCT state is sufficiently high in energy that it is not populated in the lifetime of the LE state, so the fluorescence efficiency Φ_{fl} is high ($\Phi_{fl} \sim 0.9$). In Figure 3 we show the measured Φ_{fl} values for **2** as a function of the solvent dielectric, for both pure and mixed solvents (the mixed solvent dielectric is taken as the weighted average of the dielectric constants of the two pure solvents). Shifting to toluene decreases the Φ_{fl} to ~ 0.2. This reduction in Φ_{fl} is due to the non-emissive SBCT state dropping below the LE state and rate of populating the SBCT state outcompeting fluorescence.[17] Shifting from toluene to more polar solvents further degrades Φ_{fl}, such that fluorescence is barely measurable in THF and is not observed in acetonitrile. In order to look at more subtle effects of the solvent polarity on the photophysical properties we have investigated Φ_{fl} of **2** in solvent

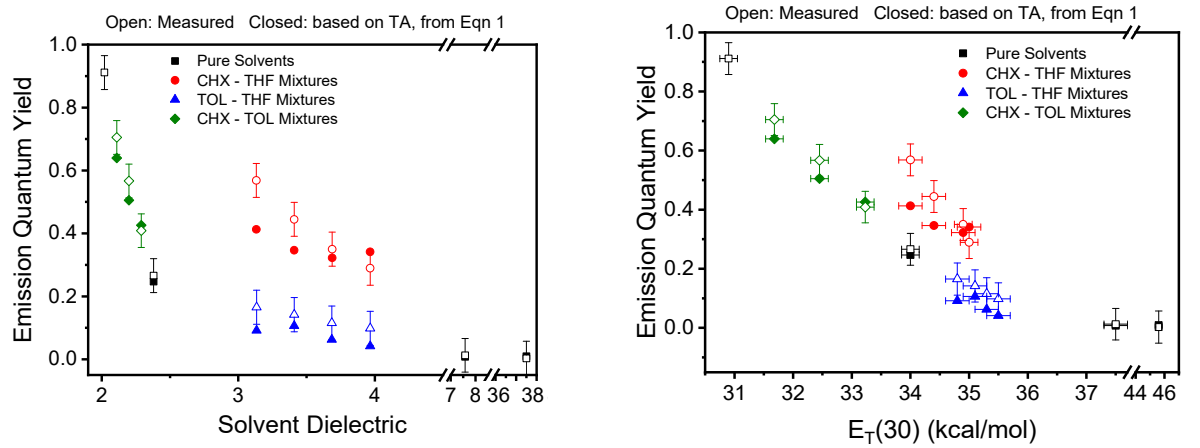

Figure 3: Photoluminescence quantum yields in a range of solvents and solvent mixtures. Both measured (closed symbols) and values calculated from the TA measurements using Eqn. 1 (closed symbols) are shown. The Φ_{fl} values are plotted versus both solvent dielectric (left) and solvent polarity, using the $E_T(30)$ scale (right).

mixtures of TOL-CHX, TOL-THF and CHX-THF. The Φ_{fl} values in solvent mixtures fall monotonically with the increasing dielectric constant of the mixture.

The Φ_{fl} for the TOL-THF and CHX-THF mixtures seem contradictory. While the solvent ratios chosen here (volume ratios were TOL-THF: 70/30 – 85/15 and CHX-THF: 65/35 – 80/20) have similar dielectric values but the measured Φ_{fl} values differ markedly. It appears that the solvent dielectric does not accurately represent the solvent effects in these two solvent mixtures. An alternate way to treat the solvent effects is to consider the polarity of the solvent, using the $E_T(30)$ scale.[25] This solvent polarity scale is based on the absorption spectrum of a charge transfer dye (Reichardt's dye: 2,6-Diphenyl-4-(2,4,6-triphenylpyridin-1-ium-1-yl)phenolate) dissolved in the solvent or a solvent mixture. Polar solvents hypsochromically shift the absorbance and less polar solvents lead to bathochromic shifts. Reichardt used this method to develop a polarity scale for common organic solvents,[26] which was later extended to solvent mixtures.[27] The absorption band used in deriving the $E_T(30)$ values for each solvent or mixture involved a phenoxide to pyridinium charge transfer, so many of the same solvent effects captured in the $E_T(30)$ scale should be similar for the electronic transitions being studied here. When the Φ_{fl} values are replotted against the

$E_T(30)$ values of the solvent mixtures overlap less (Figure 3). While there are still some contradictions at the points where the TOL-THF and CHX-THF mixtures have similar $E_T(30)$ values, the $E_T(30)$ scale captures the solvent effects better than the solvent dielectric, so we will use $E_T(30)$ in our discussion hereafter.

The Φ_{fl} values in TOL-CHX mixtures are perhaps the most interesting. In this case, the non-emissive SBCT appears to smoothly transition from not being significantly populated in the excited state to be the dominant excited state. Assuming that cyclohexane gives an LE state and toluene gives a predominantly SBCT state, this mixed solvent system allows us to find the conditions where $\Delta G° = 0$ for the LE → SBCT transition and study the rates of charge transfer and recombination as the system flips from endergonic to exergonic. In order to probe this solvent region, the rates of forward and backward charge transfer were experimentally determined using femtosecond transient absorption (TA). The TA data was fit to the three-state model proposed in Figure 1 to determine the rate constants. In order to determine the best fit for each of the samples, the fit for the bands at 380 nm and 538 nm, the absorption maxima assigned to the CT state, were monitored. Assigning error bars for the fast rate constants, k_{bet} and k_{ct}, was achieved by incrementing one value by hand, allowing the other and k_{rec} to be optimized, until the quality of the fit in the time and spectral domain was obvious as a systematic deviation in the residuals. As the time-range probed in the TA experiment is not sensitive to (k_r + k_{nr}), this value was fixed throughout to the inverse lifetime measured for the complex in cyclohexane. With the values of k_r and k_{nr} from the cyclohexane solution in hand we can use the lifetime and quantum efficiencies in other solvent systems to solve for k_{rec} (see SI, equations S3 and S4). For the pure solvents, THF and acetonitrile, we find that the TA data does not allow robust assignment of k_{ct} and k_{bet}. Even after assigning rate constants ~5 times the best fit value, no deviation in any of the time traces was detected. The ratio of these values are better pinned by the quantum yield measurement. All derived rate parameters from the TA analysis were used to construct an LE

state fluorescence quantum yield (QY) utilizing equation 1, and were found to show a good correlation with the experimentally measured values (Figure 3).[28, 29]

$$\Phi_{fl} = \frac{k_r(k_{cr}+k_{rec})}{(k_r+k_{nr})(k_{cr}+k_{rec})+k_{ct}k_{rec}} \quad \textbf{(1)}$$

Figure 4 shows the rate constants as a function of solvent dielectric for pure solvents. In high dielectric polar medium, the charge transfer state is greatly stabilized and as such, the SBCT state is populated faster than for a nonpolar medium ($k_{ct} > k_{bet}$). For the solvents acetonitrile and THF, k_{ct} is much faster than k_{bet}, so much so that the TA data can be fit even by simplifying to $k_{bet} = 0$. This indicates that for these solvents, the equilibrium established is so far to the side of charge separation that the TA experiment no longer detects the small LE population. On the other hand, the SBCT state in cyclohexane is too destabilized to support any form of SBCT so the rates for the forward reaction is assumed to be zero and the rate constants involved on the SBCT side of Figure 4 are now undefined. The mixed solvent systems allow us to probe media with dielectric constants between toluene, where $k_{ct} > k_{bet}$ and cyclohexane, where $k_{ct} < k_{bet}$, showing a clear

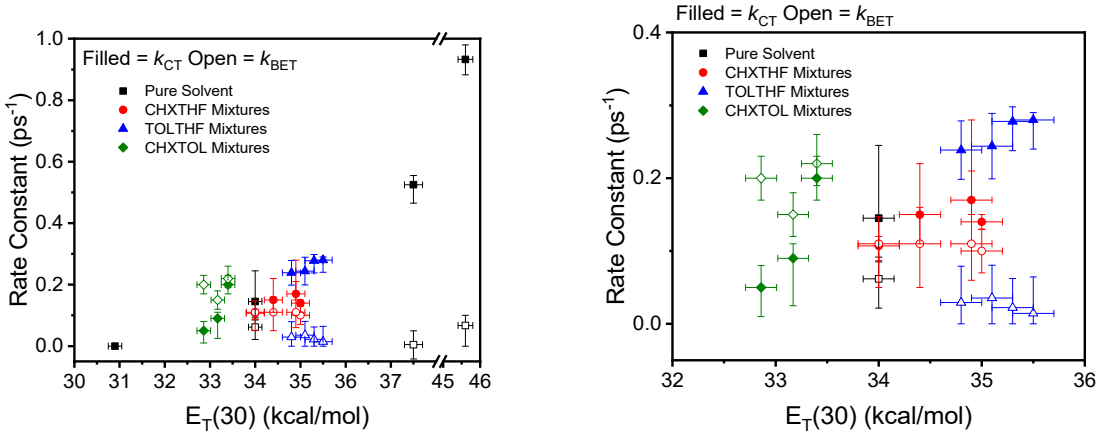

Figure 4: (left) Rate constants from TA experiments are shown for a range of solvents, from nonpolar to polar. (right) Rate constants from TA experiments are shown for both pure solvent sand solvent mixtures, focusing on the less polar solvents an mixtures. Filled symbols are k_{CT} and open symbols are k_{bet} (see Figure 1)

crossing over of the rates of forward and backward charge transfer. For a low dielectric, nonpolar medium, the backward charge transfer rate out competes the forward rate.

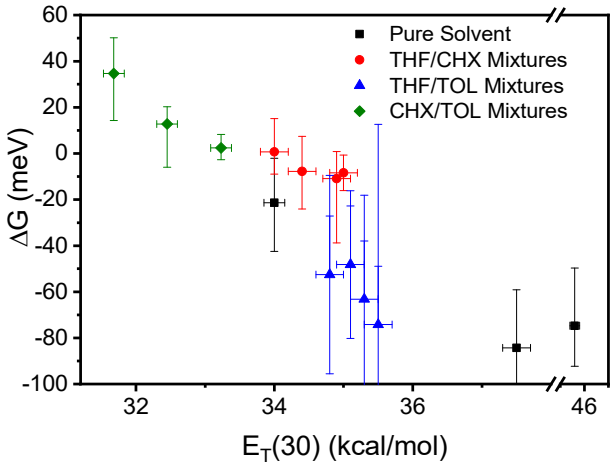

Figure 5: ΔG for the equilibrium $S_1 \rightleftarrows$ SBCT for **2** as a function of solvent $E_T(30)$. A line has been added at ΔG = 0 as a guide.

Using the values for k_{ct} and k_{bet}, the equilibrium constant and then ΔG of formation of the SBCT state from the LE state was calculated at room temperature (Figure 5). From the calculation of ΔG, we see that all mixtures of CHX and TOL lead to a positive free energy change. Thus, for a dielectric of less than toluene, the CT state is destabilized but not enough to eliminate the population of this pathway during the lifetime of fluorescence. In addition to the TOL/CHX mixtures, the 20/80 THF-CHX mixture gives a ΔG value close to zero. The $E_T(30)$ solvent parameters for the CHX-THF mixed solvent that are > 60% CHX may be impacted by the low solubility of Reichardt's dye in CHX. We are exploring other solvent models for the mixed solvents systems used here to find a better match to the experimental trends.

Modeling LE and SBCT States

The first step in the modeling studies was to optimize the geometries of the ground states for **1** and **2**. Both structures were optimized using Density Functional Theory (DFT) with the B3LYP functional and 6-31+G* basis set. A crystal structure for **1** is not available for comparison, but the geometry optimized structure of **2** matches the experimental one closely with no more than 0.03 Å difference in corresponding C-C or C-N bond lengths between the two structures. The bond lengths and angles of the dipyrrin ligands of both **1** and **2** are very similar to other BODIPY and

zinc-dipyrrin compounds, respectively. The geometry optimized structure for the *meso*-bridged **1** has a dihedral angle of 81° while the geometry optimized structure of the zinc-based compound **2** is 90°. The dipole moments for the two compounds are very similar and quite low, < 0.2 D. The DFT derived MOs of **1** and **2** (Figure 6) show the top two filled orbitals in both compounds are dipyrrin π-orbitals, and the bottom two unfilled orbitals are comprised of the dipyrrin π^*-orbitals, (see Figure 2(b) for π and π^* orbitals). The LUMO and LUMO+1 orbitals of **1** also show substantial overlap of the p_z orbitals of the two *meso*-carbons, enabled by the dihedral angle of 81°.

The key to the photophysics of these molecules is their solvent dependence. For this reason, we carried out time dependent DFT (TDDFT) calculations both in vacuum and with an implicit solvent continuum to probe the excited states. The B3LYP functional, 6-31G basis used for geometry optimization of excited states and 6-31+G* was used for electronic structure calculations with the optimized structures. These TDDFT calculations were carried out with a nonequilibrium implicit continuum solvation model. More specifically, the conductor-like screening model, COSMO,[30] is used to qualitatively model the character of the excited states in polar and nonpolar environments. COSMO is a self-consistent reaction field method. In COSMO, the solute cavity takes the shape of the molecule and is constructed using atom-centered spheres. The

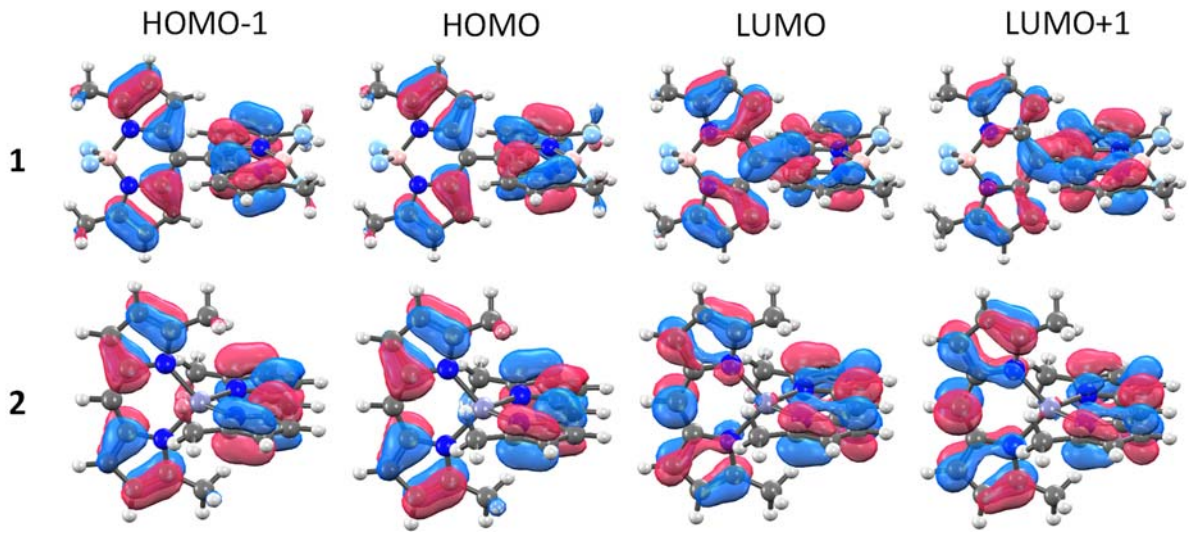

Figure 6: Molecular orbitals for **1** and **2** (DFT: B3LYP functional, 6-31+G* basis)

exact electron density of the solute is used to polarize the cavity surface into discrete point charges. COSMO also includes a correction for outlying charges, which is the part of the solute electron density that extends beyond the cavity. It should be noted, however, that COSMO is better suited for modeling high dielectric solvents. Thus, there is a sacrifice of quantitative accuracy in favor of a qualitative description.

For these COSMO modeling studies, we chose the dielectric of cyclohexane, a solvent where we see only the LE state, and acetonitrile, where the SBCT state dominates. At both low and high dielectric we see the lowest four excited states being composed of two LE states and two SBCT states. The dihedral angles between the dipyrrin planes of **1** and **2** in both the LE and SBCT states are within 1° of their ground state values, *i.e.* 81° and 90°, respectively. The natural transition orbitals (NTOs) for the LE and SBCT states for **1** and **2** are illustrated in Figure 7. The two SBCT states have a hole on one dipyrrin and an electron on the other, *i.e.* (dpy^+)Zn(dpy^-) and (dpy^-)Zn(dpy^+). The LE state consists of linear combinations of the dipyrrin localized sates on the two dipyrrins. The LE states for **1** shown in Figure 7 has NTO contributions (hole + electron) that are 70% from one dipyrrin and 30% from the other. The other LE state (not shown) has the opposite composition. The LE state does not lead to any charge build up in the molecule, and as such the LE excited states have dipole moments close to those of the ground state, 0.6 D for both **1** and **2**, with a calculated hole-electron separation < 0.1 Å. The low ground state and LE dipole moments are consistent with the low degree of solvatochromism for the absorption and emission spectra for $S_0 \rightarrow S_1$/LE. It is noteworthy that the electron NTO for the LE state of **1** shows character at <u>both</u> *meso*-carbons, consistent with the non-orthogonal orientation of the two dipyrrins. No such “bridging” character is seen for **2**. In contrast to the LE states, the SBCT states for **1** and **2** give very large dipole moments of 16.4 and 20.3 D and hole-electron separations of 3.4 and 4.4 Å, respectively, consistent with the high degree of charge separation in the SBCT state.

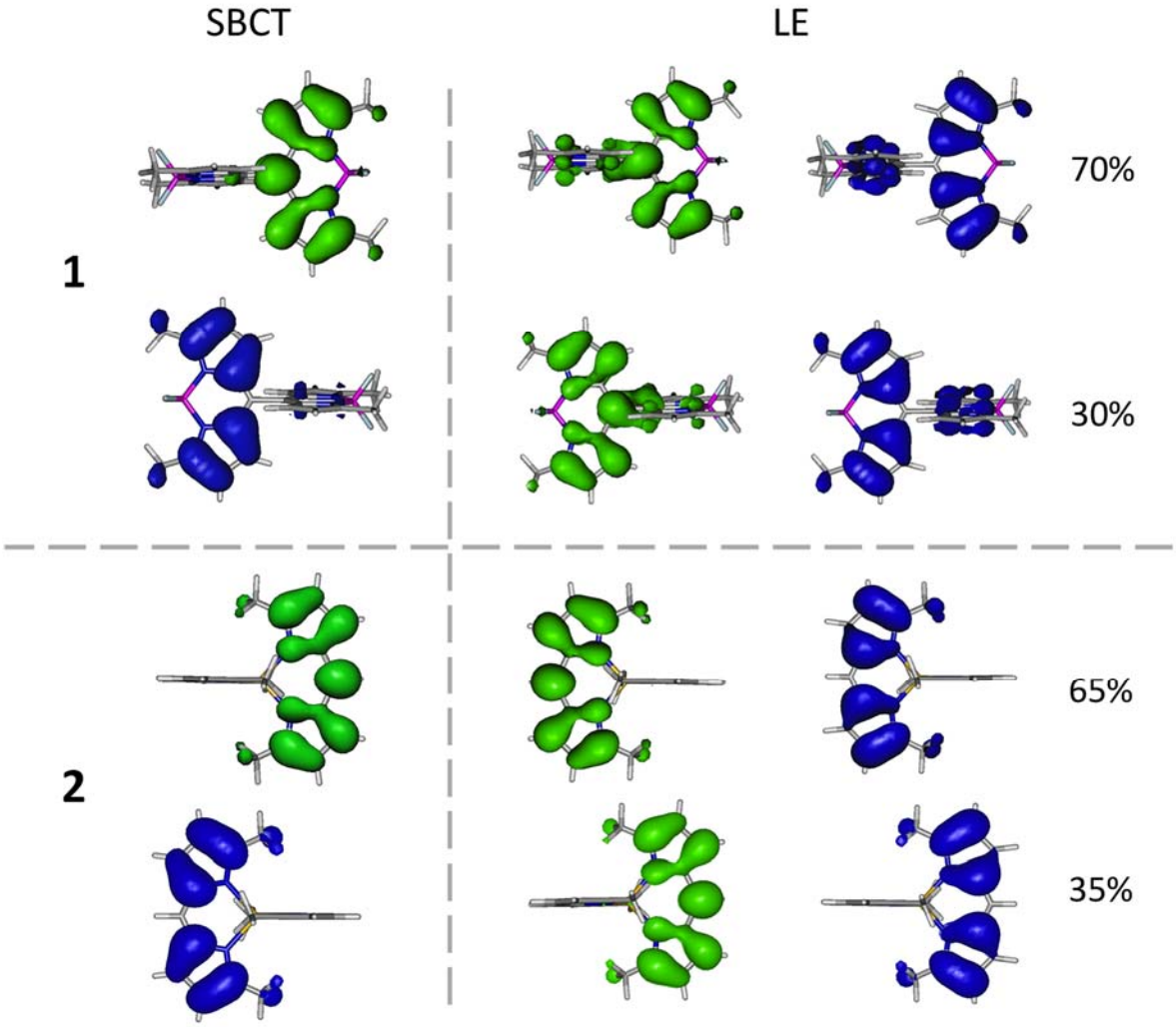

Figure 7: SBCT and LE natural transition orbitals (NTOs) for **1** and **2**. The hole orbitals are in yellow and the electron orbitals are in green.

The SBCT state of **2** shows a significant distortion of the coordination sphere around the Zn ion (Figure 8). The ground state structure of **2** has the zinc ion equally spaced between the two dipyrrin ligands, as judged by the zinc to *meso*-carbon distance (**a** and **b** in Figure 8). The Zn^{2+} ion in the SBCT structure shifts to be closer to the reduced dipyrrin and further from the oxidized one. This shift in the position of the Zn^{2+} ion is dependent on the dielectric of the continuum, with a nonpolar solvent (low dielectric) giving a 0.24 Å difference in the Zn to *meso*-carbon distances, while the shift in a high dielectric medium is 0.16 Å. This is consistent with more efficient screening of charge in the high dielectric medium. A related, albeit much smaller shift is observed

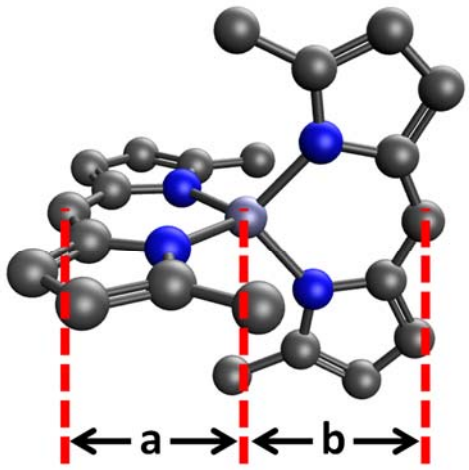

	Medium	a (Å)	b (Å)	Δ(Å)
Ground State	Gas	3.30	3.30	0
	CHX	3.30	3.30	0
	ACN	3.31	3.31	0
LE	Gas	3.30	3.30	0
	CHX	3.33	3.37	0.04
	ACN	3.33	3.36	0.03
SBCT	Gas	3.48	3.19	0.29
	CHX	3.46	3.22	0.24
	ACN	3.41	3.25	0.16

Figure 8: Geometry optimized excited state structures of **2** differ in media with different dielectric constants. The structural change here is largely a displacement of the Zn ion along the axis containing the two *meso*-carbons and the Zn ion, given by **a** and **b** above. The effect is the marked in SBCT state, where the Zn ion moves closer to the dipyrrin carrying the electron. The effect is most pronounced in nonpolar media.

for **1**. In the SBCT state for **1** he B atom is closer to the *meso*-carbon of the dipyrrin with the electron than it is to the *meso*-carbon of the dipyrrin with the hole, but the difference in distances is only 0.06 Å.

A problem with the dielectric continuum model presented above is that while the orbital make-up and transitions are consistent with the experimental data, the energies of the states are not well matched to experiment. In both high and low dielectric media the SBCT state falls below the LE in energy. This is also true in the vacuum calculations of both **1** and **2**. In order to better model the system a system with explicit solvent molecules may be needed. Moreover, It has been found that using common hybrid functionals, such as B3LYP, severely underestimate the energies of charge transfer states,[31-33] whereas long-range corrected functionals, such as CAM-B3LYP, ωPBE and ωB97xD, better match the observed energies,[34-37] and will be used in future studies of **1** and **2**. To incorporate an explicit solvent model a hybrid multiscale approach that employs classical Molecular Dynamics (MD) simulations in conjunction with the aforementioned higher

level TDDFT method is being explored. In this hybrid scheme, the formal atomic charge forcefield parameters of the chromophore are replaced by the CHELPG (Charges from Electrostatic Potentials using a Grid-based method) charges calculated for the state of interest using DFT. MD simulations are then performed with these modified parameters. Single-point TDDFT calculations are performed on snapshots of the MD equilibrated cell with the solvent atoms replaced by their corresponding CHELPG atomic charges to serve as a polarizing influence on the chromophore. The results of these studies will be reported in due course.

*Comparing the SBCT Process in meso-BODIPY (**1**) and Zn(dpy)$_2$ (**2**)*

It is instructive to compare the CT and charge recombination rates for compounds **1** and **2**, Table 1. The two compounds have very different connections between the two dipyrrin units, which lead to very different CT rates. The *meso*-bridged dimer shows a CT rate that is nearly an order of magnitude faster than the zinc dipyrrin complex. The two dipyrrins are orthogonal to each other in both structures, but the connections between them in **1** and **2** are very different. The closest contact between the two dipyrrins in **1** is 1.49 Å (C-C bond), while the closest contact between the two dipyrrins in **2** is 3.39 Å (interligand N--N contact). It is also important to stress that the differences go beyond just distance. The closest contact for **1** is at the *meso*-carbon of each dipyrrin, which is a node in the HOMO and has substantial orbital density in the LUMO (Figure 2(b)). In contrast, the closest dipyrrin-dipyrrin contacts in **2** are the nitrogen atoms of the ligand. Both the HOMO and LUMO orbitals have substantial nitrogen character, but the symmetries of the two are opposite. Twisting of the ligands away from an orthogonal relationship leads to a very weak but

	Solvent	τ_{CT} (ps)	τ_{rec} (ns)	Φ_{fl}
1	Acetonitrile	0.18	0.65	< 0.01
	Cyclohexane	--	--	0.8
2	Acetonitrile	1.1	0.9	< 0.01
	Cyclohexane	--	--	0.9

Table 1: Kinetic parameters for compounds **1** and **2**.

positive overlap for the LUMOs of the two ligands and no constructive overlap for the HOMOs.

Looking closely at the NTOs for the LE states of **1** and **2**, one can see that there is no interaction between the hole levels of the dipyrrin ligands for either compound. The same is seen for the electron levels for **2**, where the NTOs remain fully localized on single dipyrrins. However, the electron levels for **1** show a weak but positive interaction between the two dipyrrin ligands at the bridging *meso*-carbons. This is enabled by the 80° dihedral angle observed for **1**. This *meso-meso* orbital overlap is also observed in the LUMO orbitals of the ground state of **1**. A similar orbital overlap is seen for bianthryl and has been suggested as a bridge state for the LE → SBCT transition in that system.[22]In the case of **1** and **2** we postulate that it is this LE bridge state in **1** that increases the rate of charge transfer to the SBCT state by an order of magnitude, relative to charge transfer rate for **2**. In the SBCT states of both **1** and **2** no such bridge state exists; the hole and electron NTOs are fully localized in single dipyrrin ligands. Thus, it is not surprising that the recombination rates (k_{rec}) are nearly the same for both **1** and **2**., with lifetimes of 0.65 and 0.9 ns.

Another interesting comparison is that the emissive state in polar solvents of **1** is from the CT state, like 9,9'-bianthryl, meaning that radiative recombination to the ground state is weakly allowed from the SBCT state,[16] whereas **2** displays only emission from the S_1 of the BODIPY chromophore[17]. In order for recombination from the SBCT state to radiatively relax back to the ground, sufficient orbital overlap and dipolar coupling are necessary. The bridging group in **1** allows for sufficient torsion where the BODIPY chromophores can become less orthogonal, increasing orbital overlap and dipole coupling.

SBCT in **1** displays charge transfer rates like that of 9,9'-bianthryl (hundreds of femtoseconds) while in **2** the CT rate is an order of magnitude slower. Like 9,9'-bianthryl, **1** shows an electron density localized on the bridge. This implies that the BODIPY dimer complex transfers charge through-bond and may also require activation of the torsion mode as noted for bi-anthryl,

allowing for charge transfer to occur rapidly, relative to **2.** An interesting question is what moves in the LE→SBCT transition, the hole or the electron. Either carrier could be transferred to form the SBCT state. While the coupling of the two *meso*-carbons in the LUMO and electron NTO suggest it is the electron that will be transferred, the data we have presented here does not allow us to state which carrier moves unequivocally. We are currently exploring the use of ultrafast transient absorption anisotropy measurements to answer this question.

Conclusion

Marcus theory relates the rate of electron transfer to the electronic coupling between the initial and final states (H_{AB}), the solvent and molecular reorganization energies (λ) and the free energy of the electron transfer process (ΔG).[38, 39] For a case where $\Delta G = 0$, the forward and backward rates are determined by only H_{AB}, λ and the temperature. The system reported here allows us to potentially determine the electronic coupling directly, if the reorganization energy can be estimated. Experimental approaches to determining λ using the Stokes shift[40-42] are not useful since the SBCT state does not emit. We could alternatively estimate λ theoretically, however, the dielectric continuum calculations discussed above are not accurate enough for this. We are currently carrying out QMMM modeling studies with explicit solvent molecules, at a markedly high level of quantum mechanical theory for the excited chromophores than used above. Deriving a reliable λ value in mixed solvent systems with this QMMM approach may be problematic, but should give us good values in pure solvents. Thus, we will use QMMM derived λ and our experimental values for ΔG and k_{CT} in in toluene, THF and acetonitrile to measure the electron coupling in each of these solvents. Solvent dependent structural differences between the LE and SBCT structures will affect λ and may impact the electronic coupling as well.

Methods

Compounds **1** and **2** were prepared by literature procedures.[16, 17]

Photoluminescence Quantum Yield Measurements:

All absorption measurements were taken on a Cary 50 UV-VIS. Steady state relative QY measurements were performed using a fluorescence QY standard. The standard used was fluorescein in 0.1 M NaOH. Each of the pure solvents and solvent mixtures were tested. First, zDIP2 was dissolved in its respective solvent or solvent mixture to obtain an absorbance of near or below 0.1OD at 496nm, the excitation wavelength used in fluorescence measurements in a cuvette with a pathlength of 4mm. This wavelength was chosen because it was the wavelength used for fluorescein, the quantum yield reference as well as being close to the maximum absorption of zDIP2. The emission spectra wereas taken. Fluorescence spectra were obtained on a Horiba Jobin Yvon FluoroMax-3 fluorimetor using DataMax v2.2 software. The parameters used for fluorescence measurements were 0.25 nm interval, 1 nm slit width, and 100 ms integration time. The reference fluorescein was run under the same absorption and emission conditions as **21**. The total area of the fluorescence spectrum was then calculated after subtracting off the dark background. The fluorescence QY in reference to fluorescein was calculated using equation 2:

$$QY_S = \frac{E_S \cdot f_R \cdot n_S^2}{E_R \cdot f_S \cdot n_R^2} \cdot QY_R \qquad \textbf{(2)}$$

Here, S and R subscripts refer to sample and reference respectively, E_x for the area under the emission curve, n_x for the refractive index of the solvent or mixed solvent, QY_R for the reference QY of fluorescein (95%)[5] and f_x for the absorption correction factor where $f_x = 1 - 10^{-A_x}$ Where A_x is the absorbance at the excitation wavelength used in the emission experiment. The refractive indices of the pure solvents were taken from literature and the solvent mixture refractive indices

were just calculated as a weighted sum of the pure solvents according to, the Arago-Biot equation.[43, 44] This is not the ideal case for a binary mixture but the other errors in the QY measurement due to absorbance and fluorescence are assumed to be larger.

Ultrafast Transient Absorption Spectroscopy

Pump probe experiments were done after taking the output of a Ti:sapphire regenerative amplifier (Coherent Legend Elite, 1kHz, 3.8mJ, 35fs) with both single color pumping and broadband probing the sample. For the pure solvents and the CHXTHF mixtures, the excitation pulses were generated from a type-II OPA (Spectra Physics OPA-800CF), centered around 500nm with a spectral bandwidth of 10-13 nm.

For the TOLTHF and CHXTOL mixtures, a homebuilt noncolinear optical parametric amplifier (NOPA) was used to pump the sample instead of the commercial OPA mentioned previously. Here the residual 800 nm pump from the amplifier was sent through a type I BBO to frequency double the pump which was then combined with a white light continuum generated by a sapphire disk to generate 500 nm. The signal output was then sent through a double prism compressor to temporally shorten the pulses.

The probe pulses were generated after taking the residual 800 nm amplifier output, passing it through a λ/2 waveplate, and focusing it onto a rotating 2mm CaF_2 window. This white light supercontinuum (320 nm to 950 nm) was then collimated and focused at the sample using a pair off-axis parabolic mirrors. After passing through the sample, the supercontinuum was then collimated and focused at the slit of a Czerny-Turner monochromator. The probe was then dispersed onto a 256- pixel silicon diode array (Hamamatsu) for multiplexed detection of the probe. The probe polarization was set at magic angle (54.7^{o}) with respect to the pump to avoid any contribution to the observed signal from orientational dynamics.

After passing through a chopper tuned to 500 Hz, the pump was focused before the sample using a 25 cm lens. The cross-correlation of the pump and probe pulses through a 1 mm quartz cuvette was determined to have a <150 fs instrument response for the OPA and 80fs for the NOPA. The pump was blocked after exciting the sample.

Theoretical methods

All Density Functional Theory (DFT) calculations reported in this work were performed using the Q-Chem (5.1) software package[30]. Ground state geometries of the molecules were optimized at the B3LYP/6-31+G* level in vacuum and using the conductor-like screening model[45] (COSMO) for cyclohexane and acetonitrile. Vertical excitation energies were computed using TDDFT on the corresponding ground state optimized structures in vacuum and using the COSMO linear response solvation approach in the non-equilibrium limit. Excited state geometry optimization calculations were performed using TDDFT at the B3LYP/6-31G level.

Conflicts of Interest

There are no conflicts of interest to report.

Acknowledgements

The authors would like to acknowledge the Office of Basic Energy Sciences at the Department of Energy (DE-SC0016450) for supporting this work. The authors have no competing financial interest in this work. The authors would also like to acknowledge Kyro Grace for performing the first set of photoluminescence experiments.

References

1. J. R. Norris, M. E. Druyan and J. J. Katz, *J. Am. Chem. Soc.*, 1973, **95**, 1680-1682.
2. W. W. Parson, A. Scherz and A. Warshel, in *Antennas and Reaction Centers of Photosynthetic Bacteria*, ed. M. E. Michel-Beyerle, Springer-Verlag, Berlin, 1985, pp. 122-130.
3. W. Rettig, *Angewandte Chemie-International Edition In English*, 1986, **25**, 971-988.
4. A. N. Bartynski, M. Gruber, S. Das, S. Rangan, et al., *J. Am. Chem. Soc.*, 2015, **137**, 5397-5405.
5. Z. R. Grabowski, K. Rotkiewicz and W. Rettig, *Chem. Rev.*, 2003, **103**, 3899-4031.
6. J. M. Giaimo, A. V. Gusev and M. R. Wasielewski, *J. Am. Chem. Soc.*, 2002, **124**, 8530-8531.
7. J. M. Giaimo, J. V. Lockard, L. E. Sinks, A. M. Scott, T. M. Wilson and M. R. Wasielewski, *J. Phys. Chem. A*, 2008, **112**, 2322-2330.
8. F. Schneider and E. Lippert, *Berichte Der Bunsen-Gesellschaft Fur Physikalische Chemie*, 1968, **72**, 1155-1160.
9. F. Schneider and E. Lippert, *Berichte Der Bunsen-Gesellschaft Fur Physikalische Chemie*, 1970, **74**, 624-630.
10. F. C. Grozema, M. Swart, R. W. J. Zijlstra, J. J. Piet, L. D. A. Siebbeles and P. T. van Duijnen, *J. Am. Chem. Soc.*, 2005, **127**, 11019-11028.
11. S. Das, W. G. Thornbury, A. N. Bartynski, M. E. Thompson and S. E. Bradforth, *The Journal of Physical Chemistry Letters*, 2018, **9**, 3264-3270.
12. S. Duman, Y. Cakmak, S. Kolemen, E. U. Akkaya and Y. Dede, *The Journal of Organic Chemistry*, 2012, **77**, 4516-4527.
13. L. Wang, J. Cao, J.-w. Wang, Q. Chen, A.-j. Cui and M.-y. He, *RSC Adv.*, 2014, **4**, 14786-14790.
14. Y. Cakmak, S. Kolemen, S. Duman, Y. Dede, et al., *Angew. Chem. Int. Ed.*, 2011, **50**, 11937-11941.
15. A. B. Nepomnyashchii and A. J. Bard, *Acc. Chem. Res.*, 2012, **45**, 1844-1853.
16. M. T. Whited, N. M. Patel, S. T. Roberts, K. Allen, P. I. Djurovich, S. E. Bradforth and M. E. Thompson, *Chem. Commun.*, 2012, **48**, 284-286.
17. C. Trinh, K. O. Kirlikovali, S. Das, M. E. Ener, H. B. Gray, P. I. Djurovich, S. Bradforth and M. E. Thompson, *The Journal of Physical Chemistry C*, 2014, DOI: 10.1021/jp506855t.
18. I. V. Sazanovich, C. Kirmaier, E. Hindin, L. H. Yu, D. F. Bocian, J. S. Lindsey and D. Holten, *J. Am. Chem. Soc.*, 2004, **126**, 2664-2665.
19. C. Trinh, K. Kirlikovali, S. Das, M. E. Ener, H. B. Gray, P. Djurovich, S. E. Bradforth and M. E. Thompson, *The Journal of Physical Chemistry C*, 2014, **118**, 21834-21845.
20. J. J. Piet, W. Schuddeboom, B. R. Wegewijs, F. C. Grozema and J. M. Warman, *J. Am. Chem. Soc.*, 2001, **123**, 5337-5347.
21. S. N. Smirnov and C. L. Braun, *Rev. Sci. Instrum.*, 1998, **69**, 2875-2887.
22. T. Takaya, H. O. Hamaguchi and K. Iwata, *J. Chem. Phys.*, 2009, **130**, 014501.
23. K. Nishiyama, T. Honda and T. Okada, *Acta Phys. Pol., A*, 1998, **94**, 847-856.
24. S. Hashimoto, A. Yabushita, T. Kobayashi, K. Okamura and I. Iwakura, *Chem. Phys.*, 2018, **512**, 128-134.
25. C. Reichardt, *Chem. Rev.*, 1994, **94**, 2319-2358.
26. C. Reichardt, *Angewandte Chemie International Edition in English*, 1979, **18**, 98-110.
27. P. M. E. Mancini, A. Terenzani, M. G. Gasparri and L. R. Vottero, *J. Phys. Org. Chem.*, 1995, **8**, 617-625.
28. D. Veldman, S. M. Chopin, S. C. Meskers and R. A. Janssen, *J. Phys. Chem. A*, 2008, **112**, 8617-8632.

29. W. R. Ware, D. Watt and J. D. Holmes, *J. Am. Chem. Soc.*, 1974, **96**, 7853-7860.
30. Y. H. Shao, Z. T. Gan, E. Epifanovsky, A. T. B. Gilbert, et al., *Mol. Phys.*, 2015, **113**, 184-215.
31. A. Dreuw, J. L. Weisman and M. Head-Gordon, *J. Chem. Phys.*, 2003, **119**, 2943-2946.
32. A. Dreuw and M. Head-Gordon, *J. Am. Chem. Soc.*, 2004, **126**, 4007-4016.
33. D. J. Tozer, R. D. Amos, N. C. Handy, B. O. Roos and L. Serrano-Andres, *Mol. Phys.*, 1999, **97**, 859-868.
34. J. D. Chai and M. Head-Gordon, *J. Chem. Phys.*, 2009, **131**.
35. D. Jacquemin, E. A. Perpete, G. E. Scuseria, I. Ciofini and C. Adamo, *J. Chem. Theory Comput.*, 2008, **4**, 123-135.
36. D. Jacquemin, V. Wathelet, E. A. Perpete and C. Adamo, *J. Chem. Theory Comput.*, 2009, **5**, 2420-2435.
37. T. Tsuneda and K. Hirao, *Wiley Interdisciplinary Reviews-Computational Molecular Science*, 2014, **4**, 375-390.
38. R. A. Marcus, *Angewandte Chemie International Edition in English*, 1993, **32**, 1111-1121.
39. in *Prog. Inorg. Chem.*, DOI: doi:10.1002/9780470166314.ch9.
40. E. L. Mertz, V. A. Tikhomirov and L. I. Krishtalik, *The Journal of Physical Chemistry A*, 1997, **101**, 3433-3442.
41. M. Halder, S. Datta, P. Bolel, N. Mahapatra, S. Panja, H. Vardhan, S. Kayal, D. K. Khatua and I. Das, *Analytical Methods*, 2016, **8**, 2805-2811.
42. W. W. Parson, *Modern Optical Spectroscopy: With Exercises and Examples from Biophysics and Biochemistry*, Springer Berlin Heidelberg, 2015.
43. S. C. T. Bhatia, N.; Dubey, G. P. , *Indian J. Chem. - Sect. A Inorganic, Phys. Theor. Anal. Chem.* , 2002, **41**, 266-269.
44. S. O. Isehunwa, E. B. Olanisebe, O. O. Ajiboye and S. A. Akintola, *African Journal of Pure and Applied Chemistry*, 2015, **10**, 58-64.
45. A. Klamt and G. Schuurmann, *Journal of the Chemical Society-Perkin Transactions 2*, 1993, DOI: 10.1039/p29930000799, 799-805.

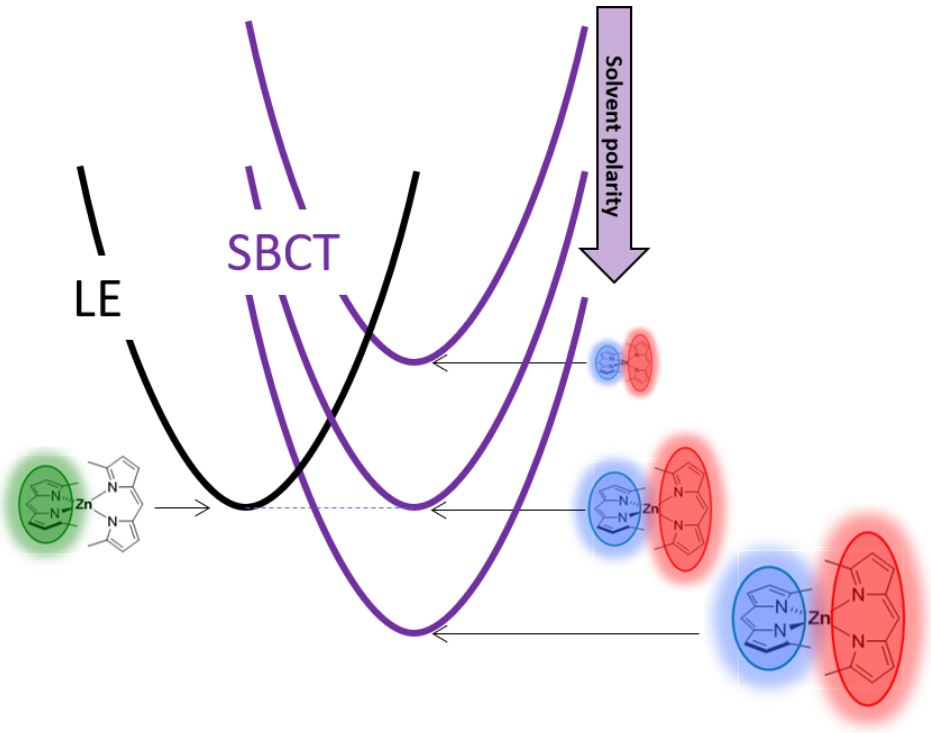

150x114mm (150 x 150 DPI)